Report

TERT activates endogenous retroviruses to promote an immunosuppressive tumour microenvironment

Jian Mao[†], Qian Zhang[†], Yaxiang Wang, Yang Zhuang, Lu Xu, Xiaohe Ma, Di Guan, Junzhi Zhou, Jiang Liu, Xiaoying Wu, Qian Liang, Miao Wang & Yu-Sheng Cong*

Abstract

Telomerase plays a pivotal role in tumorigenesis by both telomere-dependent and telomere-independent activities, although the underlying mechanisms are not completely understood. Using single-sample gene set enrichment analysis (ssGSEA) across 9,264 tumour samples, we observe that expression of telomerase reverse transcriptase (TERT) is closely associated with immunosuppressive signatures. We demonstrate that TERT can activate a subclass of endogenous retroviruses (ERVs) independent of its telomerase activity to form double-stranded RNAs (dsRNAs), which are sensed by the RIG-1/MDA5-MAVS signalling pathway and trigger interferon signalling in cancer cells. Furthermore, we show that TERT-induced ERV/interferon signalling stimulates the expression of chemokines, including CXCL10, which induces the infiltration of suppressive T–cell populations with increased percentage of CD4^{+} and FOXP3^{+} cells. These data reveal an unanticipated role for telomerase as a transcriptional activator of ERVs and provide strong evidence that TERT-mediated ERV/interferon signalling contributes to immune suppression in tumours.

Introduction

Telomerase reverse transcriptase (TERT), the catalytic subunit of telomerase, plays a critical role in cancer formation by maintaining telomere homeostasis and the cellular proliferation potential (Blasco, 2005). Most human somatic cells have undetectable telomerase activity due to transcriptional repression of *TERT* during embryonic development. However, *TERT* is universally reactivated during tumorigenesis and has been considered a hallmark of cancer cells (Cong *et al*, 2002). Recent studies have shown that in addition to telomere maintenance, TERT is also involved in several cellular

processes independent of its telomerase activity, including the WNT/β-catenin signalling pathway (Park *et al*, 2009), NF-κB signalling pathway (Ghosh *et al*, 2012; Ding *et al*, 2013), and epithelial–mesenchymal transition (Liu *et al*, 2013). However, the underlying mechanisms of TERT in tumorigenesis are not completely understood.

ERVs, which integrated into the genome of mammals millions of years ago via exogenous retroviral infections of germ cells (Feschotte & Gilbert, 2012), represent ~8% of the human genome (Lander *et al*, 2001). Although it is generally believed that most of ERVs do not encode proteins due to drastic genetic alterations (Vargiu *et al*, 2016), recent studies have shown that some coding-competent ERVs are implicated in embryonic development (Mi *et al*, 2000) and diseases, including neurological diseases (Küry *et al*, 2018) and cancer (Matteucci *et al*, 2018). However, the relationship between TERT and ERVs in tumorigenesis is not known.

In the current study, we found that expression of *TERT* is closely associated with immunosuppressive signatures. We then demonstrated that TERT can trigger interferon signalling by activating a subclass of ERVs independent of its telomerase activity in cancer cells. The TERT-induced ERV/interferon signalling stimulated the expression of chemokines, such as CXCL10, which induced suppressive T-cell infiltration, contributing to the establishment of immunosuppressive tumour microenvironment.

Results and Discussion

TERT expression is associated with immunosuppressive signatures

To comprehensively characterize genome-wide expression signatures associated with *TERT* expression in cancer cells, we divided 9,264 tumour samples across 24 cancer types derived from The Cancer Genome Atlas (TCGA) (Rahman *et al*, 2015) into two groups (*TERT*[high] and *TERT*[low]) based on their *TERT* expression levels. Using single-sample gene set enrichment analysis (ssGSEA) for immune cell infiltration (Bindea *et al*, 2013; Charoentong *et al*, 2017), we observed that *TERT* expression was closely associated with immunosuppressive signatures, at the top of which was type

---

Key Laboratory of Aging and Cancer Biology of Zhejiang Province, Hangzhou Normal University School of Basic Medical Sciences, Hangzhou, China
*Corresponding author. Tel: +86-571-2886-1693; E-mail: yscong@hznu.edu.cn
[†]These authors contributed equally to this work

2 T helper cells (Th2 cells), followed by regulatory T cells (Treg cells), CD56dim natural killer cells (NK CD56dim cells), and myeloid-derived suppressor cells (MDSCs) (Jia *et al*, 2018) (Fig 1A). The heat map of ssGSEA for TCGA tumour samples grouped into *TERT* high/low categories confirmed robust and significant association of *TERT*high tumours with these immunosuppressive signatures (Fig 1B). This indicated that *TERT* may participate in immune suppressive function.

Expression of TERT triggers interferon response

To assess whether TERT is involved in immune suppressive function independent of telomere maintenance, we ectopically expressed TERT-WT or catalytically inactive mutant TERT-K626A (Ding *et al*, 2013) in U2OS (telomerase-negative) and HeLa (telomerase-positive) cells. RNA-seq and Gene Ontology (GO) analysis of the U2OS cells revealed that the expression of TERT induced significant enrichments of GO terms associated with viral defence and type I interferon response (Fig EV1A). Furthermore, ssGSEA analysis indicated that both TERT-WT and TERT-K626A induced interferon response (Fig EV1B). Consistently, expression of a panel of genes involved in interferon response, including *IFNB1*, *ISG15*, *ISG20*, *IFI27*, *IFI35*, *IFI44*, *OASL*, and *CXCL10*, were activated by both TERT-WT and TERT-K626A (Fig 1C and D). The expression of these genes has been reported to be tightly associated with immunosuppressive microenvironment (Cañadas *et al*, 2018; Guldner *et al*, 2020). Similar results were also obtained in HeLa cells (Fig 1D). Interestingly, we observed that RNA cytosolic sensor genes (*DDX41*, *DDX58/RIG-1*, and *IFIH1/MDA5*) were also co-ordinately upregulated (Fig 1C and D). Considering that DDX58/RIG-1 and IFIH1/MDA5 are the key viral RNA sensing proteins in the cytoplasm and that their activation induces downstream signalling via MAVS, TBK1, and IRF3 (Hur, 2019), we speculated that TERT may trigger the RIG-1/MDA5-MAVS signalling pathway. Using western blot analysis, we confirmed the activation of TBK1 (pTBK1 Ser172) and IRF3 (pIRF3 Ser396) signalling in U2OS and HeLa cells, which act downstream of the MAVS signalling pathway, upon ectopic expression of TERT-WT or TERT-K626A (Fig 1E). Furthermore, enzyme-linked immunosorbent assays (ELISA) revealed that levels of IFNβ and CXCL10 increased in the culture supernatant of U2OS and HeLa cells ectopically expressing TERT-WT or TERT-K626A (Fig 1F). In

addition, knockdown of TERT by siRNAs in HeLa and HCT116 cells resulted in downregulated expression of interferon-related genes (Fig 1G), reduced phosphorylation of TBK1 and IRF3 (Fig 1H), and significantly decreased level of CXCL10 in culture supernatant (Fig 1I). These data suggest that TERT is involved in interferon response.

TERT triggers interferon response via induction of dsRNAs transcribed from ERVs

Studies have shown that cellular double-stranded RNA (dsRNA) can activate viral cytosolic RNA sensors (Hur, 2019). We reasoned that activation of viral cytosolic RNA sensors by TERT might be due to increase in dsRNA levels in cells. By immunofluorescence analysis with dsRNA-specific antibody (J2), we observed that both TERT-WT and TERT-K626A induced dsRNA expression (Fig 2A). As active ERVs can fold into dsRNA secondary structures that can trigger interferon response (Chiappinelli *et al*, 2015; Roulois *et al*, 2015), we analysed the expression of ERVs in U2OS cells. Results revealed that a large number of ERVs were upregulated by TERT-WT or TERT-K626A expression (Fig 2B). We named these TERT-activated ERVs TA-ERVs. The top upregulated TA-ERVs are listed in Fig 2C, which included MLT1O-int, LTR69, LTR38-int, MER88, MER92C, and MLT1G1-int. The activation of these ERVs by TERT-WT or TERT-K626A were further confirmed using quantitative reverse transcription polymerase chain reaction (RT–qPCR) in U2OS and HeLa cells (Fig 2D). Conversely, knockdown of TERT led to reduced expression of TA-ERVs in HeLa and HCT116 cells (Fig 2E). To exclude the effects of telomere elongation associated with TERT ectopic expression, we determined the telomere lengths in U2OS and HeLa cells ectopically expressing TERT-WT or TERT-K626A using qPCR analysis (T/S ratio) (Gil & Coetzer, 2004). The results showed that transient transfection of TERT-WT or TERT-K626A did not significantly affect telomere length (Fig EV1C), confirming that the activation of ERVs by TERT is independent of telomere lengths.

To ascertain the interferon response and TA-ERVs activation are related to TERT specifically, we have ectopically expressed TERT in U2OS and human fibroblasts WI38 cells (both telomerase-negative) at the levels comparable to that of HeLa cells by using doxycycline (Dox)-inducible system (Fig EV1D). We found that both interferon-related genes and TA-ERVs were upregulated (Figs 2F and EV1E),

Figure 1. TERT expression is associated with immunosuppressive signatures and triggers interferon response.

A   Scatterplot representing differences in ssGSEA immune signatures in *TERT*high versus *TERT*low tumours (*n* = 4,632 tumours in each group) across TCGA. −log10(padj) for enrichment of ssGSEA immune signatures in *TERT*high versus *TERT*low tumours is shown on the *y*-axis. Signatures more highly represented in *TERT*high tumours are shown on the right, while those in *TERT*low tumours are shown on the left.

B   Heat map for ssGSEA of immune signatures in *TERT*high and *TERT*low tumours (*n* = 4,632 tumours in each group) across TCGA. Th1, Th2, Th17: T helper 1, 2, 17 cells, Tcm: central memory T cells, Tem: effector memory T cells, Tgd: gamma delta T cells, TFH: follicular helper T cells, Treg: regulatory T cells, MDSC: myeloid-derived suppressor cells, DC: dendritic cells, aDC: activated DCs, iDC: immature DCs, pDC: plasmacytoid DCs, NK cells: natural killer cells.

C   Heat map of interferon-related genes in U2OS cells with TERT-WT or TERT-K626A ectopic expression.

D–F   RT–qPCR analysis of interferon-related genes (D), western blot analysis of TERT, TBK1, pTBK1, IRF3, pIRF3, and GAPDH levels (E), and ELISA of IFNβ and CXCL10 in culture supernatant (F) in U2OS and HeLa cells ectopically expressing TERT-WT or TERT-K626A.

G–I   RT–qPCR analysis of interferon-related genes (G), western blot analysis of TERT, TBK1, pTBK1, IRF3, pIRF3, and GAPDH levels (H), and ELISA analysis of CXCL10 in culture supernatant (I) in HeLa and HCT116 cells with TERT knockdown.

Data information: Data represent mean ± SEM of three biological replicates (D, F, G and I). *$P < 0.05$, **$P < 0.01$, ***$P < 0.001$, ns, not significant. One-way ANOVA with Fisher's LSD tests was used for (D) and (F), unpaired two-tailed Student's *t*-tests were used for (G) and (I). Relative levels of pTBK1 and pIRF3 were quantified with ImageJ software and normalized to GAPDH, as indicated at the bottom of the blot (E and H).
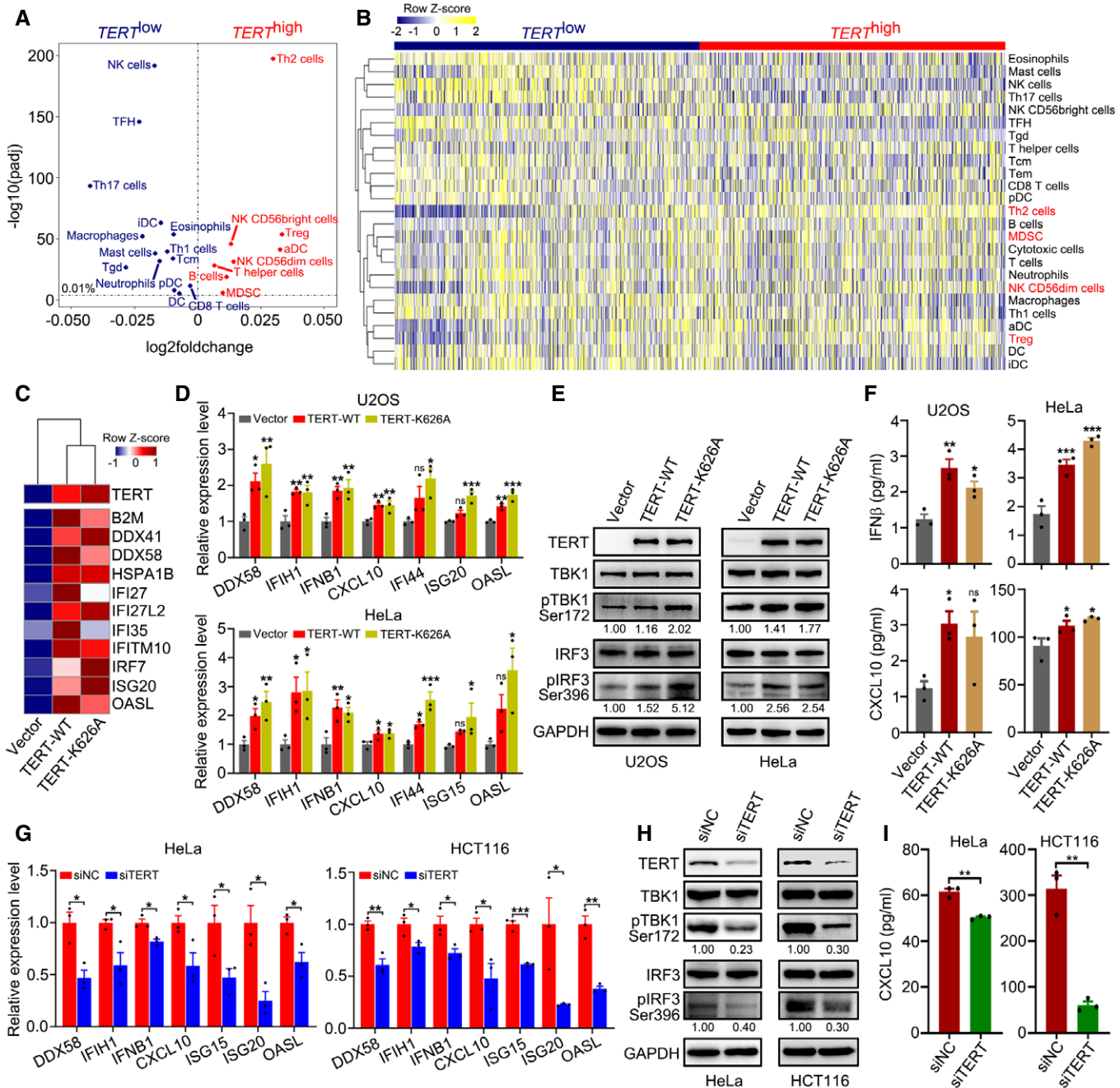
Source data are available online for this figure.

Figure 1.

TBK1 and IRF3 were activated (Figs 2G and EV1F), and levels of IFNβ and CXCL10 increased in culture supernatant (Figs 2H and EV1G), upon induction of TERT expression. These results support that TERT regulates interferon response and TA-ERVs expression.

To further verify that dsRNAs are formed from TA-ERVs, we precipitated dsRNA from U2OS cells ectopically expressing TERT-WT or TERT-K626A using dsRNA-specific antibody (J2) and performed strand-specific RNA-seq (dsRIP-seq). The results of dsRIP-seq showed that both sense and anti-sense transcripts of these TA-ERVs were expressed at comparable levels (Fig 3A). In addition, using strand-specific RT–qPCR analysis, we detected bidirectional transcription producing sense and anti-sense

transcripts for MLT1O-int, LTR69, LTR38-int, MER88, MER92C, and MLT1G1-int, but not for β-actin, in U2OS and HeLa cells ectopically expressing TERT-WT or TERT-K626A (Fig 3B). These data suggest that TERT can activate ERVs to form dsRNA via bidirectional transcription, thereby triggering interferon response.

TERT expression is significant positive correlation with TA-ERVs in tumours

To further validate our data, we analysed the expression of *TERT* and ERVs in 103 tumour samples across 11 cancer types available
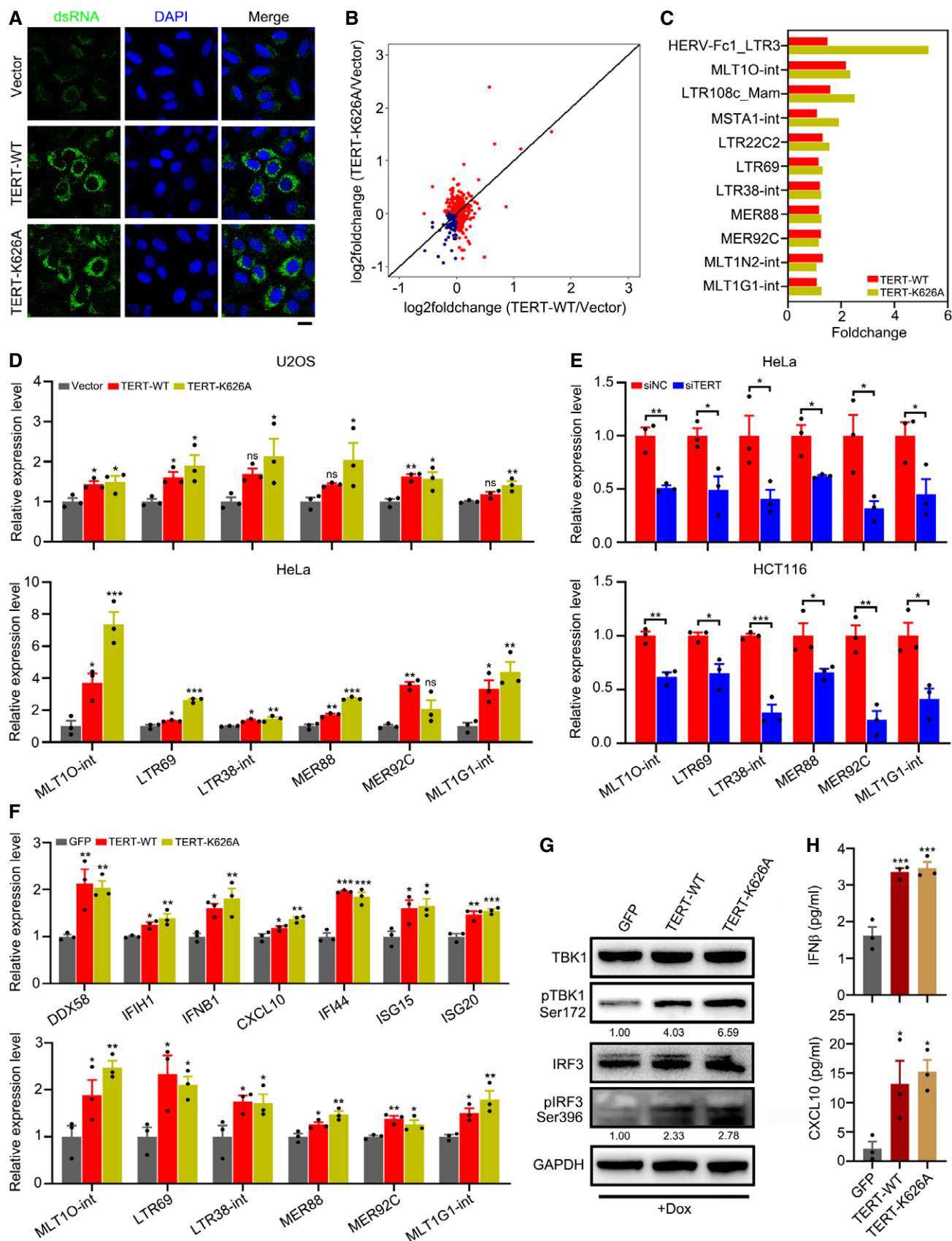
Figure 2.

from the Gene Expression Omnibus (GEO) and observed significant positive correlation between *TERT* and TA-ERVs (Fig 3C). In addition, we analysed the expression of *TERT* and TA-ERVs in different human tissues from the GEO. Results indicated that *TERT* is expressed more in immune tissues, including the appendix, bone marrow, lymph node, and thymus (Fig EV2A). Concomitantly, the TA-ERVs are also highly expressed in these tissues (Fig EV2A), suggesting that the TERT-ERVs axis is involved in immune function.
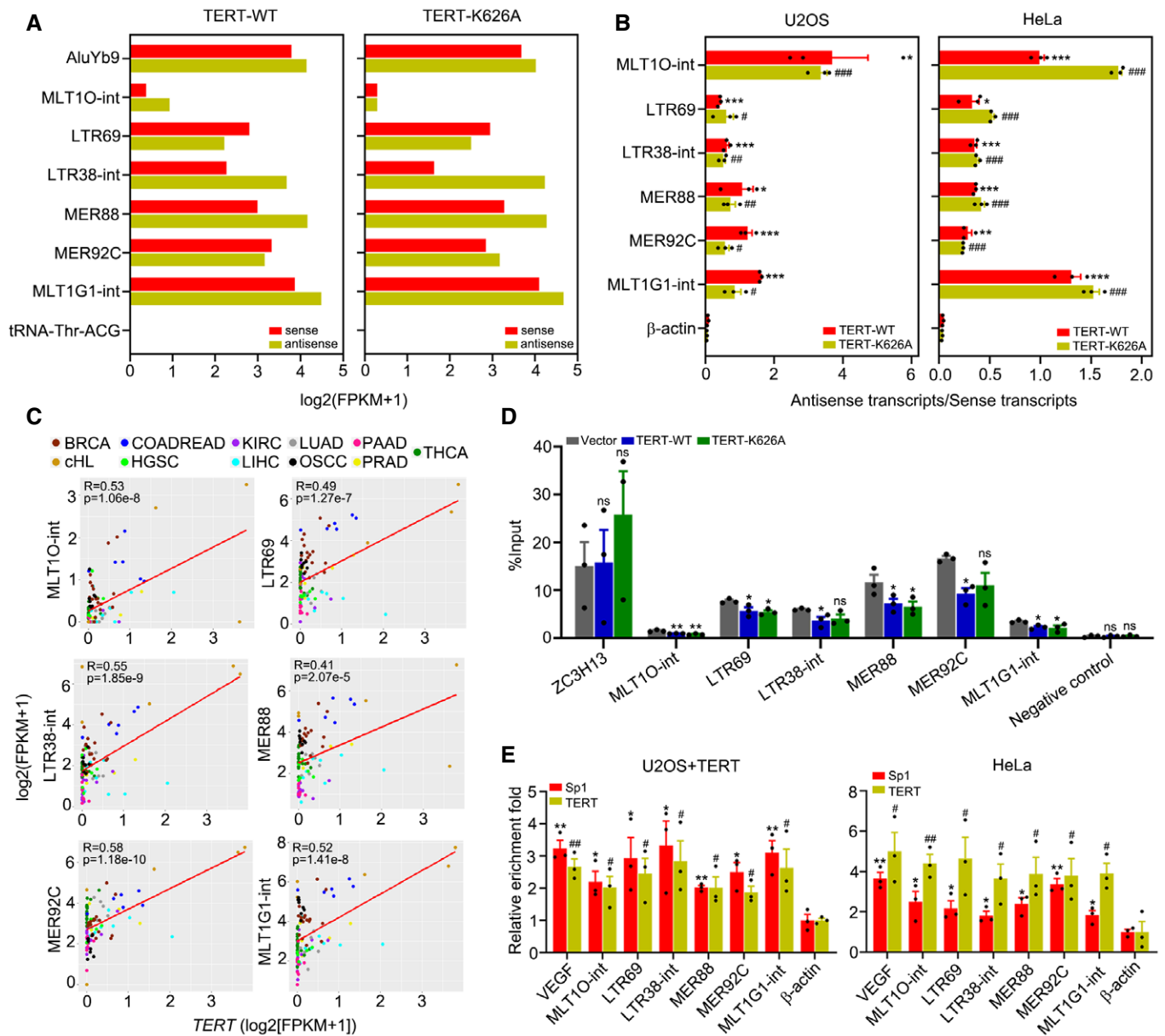
TERT activates ERVs by interacting with Sp1

In general, ERVs are silenced by the host, and DNA methylation plays an important role in preserving the silent state of ERVs (Groh & Schotta, 2017). However, ERVs can be derepressed due to reduced DNA methylation in cancer cells (Strissel *et al*, 2012; Espinet *et al*, 2021). Using methylated DNA immunoprecipitation (MeDIP)-qPCR, we observed that the methylation levels of MLT1O-int, LTR69, LTR38-int, MER88, MER92C, and MLT1G1-int indeed decreased in HeLa cells ectopically expressing TERT-WT or TERT-K626A (Fig 3D), which is consistent with the transcriptionally active status of these ERVs. Therefore, we analysed the sequences of the significantly upregulated TA-ERVs and identified the motif of the transcription factor Sp1 in the TA-ERV sequences (Fig EV2B). Sp1 has been reported to bind to ERVs and protect them from methylation, thereby activating the ERVs (Manghera & Douville, 2013). In line with these observations, we have previously demonstrated that TERT can interact with Sp1 to activate vascular endothelial growth factor (VEGF) expression (Liu *et al*, 2016). Our analyses of ChIP-seq data from the GEO indicated that both TERT and Sp1 can bind to the genomic sites of ERV families, including ERV1, ERVK, ERVL, and ERVL-MaLR (Fig EV2C). Therefore, we performed ChIP-qPCR analysis using antibodies against TERT and Sp1 in U2OS cells ectopically expressing TERT (U2OS+TERT) and in HeLa cells, and the results showed that TERT and Sp1 share a common binding sites on TA-ERVs (Fig 3E). Furthermore, Sp1 knockdown compromised TERT-mediated ERV expression, as revealed by RNA-seq analysis (Fig EV2D–F). These data indicate that TERT can activate ERV expression by interacting with transcription factor Sp1.

Deletion of *Tert* leads to decreased ERV expression and compromised interferon response in mice

As demonstrated above, TA-ERVs can form dsRNA to trigger interferon response. To determine whether TERT participated in interferon response *in vivo*, we compared WT mice with G1 *Tert$^{-/-}$* mice that have no apparent telomere dysfunction (Liu *et al*, 2000). We first analysed the expression levels of murine ERVs in the blood of these mice using RT–qPCR and observed that expression of MuERVL, IAP, MusD (also known as ETnERV), and MMERGLN was reduced in G1 *Tert$^{-/-}$* mice compared to WT mice (Fig 4A). We then analysed the expression levels of *Tert* and ERVs in different tissues of mice from the GEO and found a positive correlation between *Tert* and MuLV-int, MMETn-int, ETnERV-int and MMERGLN expression in different tissues of mice (Fig EV3A). Interestingly, *Tert* and ERVs were synchronously expressed at higher levels in immune tissues, such as the spleen and thymus, in agreement with the observation in human tissues (Figs EV2A and EV3A). Furthermore, we analysed the expression of ERVs in the livers of WT and G1 *Tert$^{-/-}$* mice treated with ENU (a reagent that can activate ERVs in mouse (Wu *et al*, 2012)) or saline (control) using RT–qPCR. The results showed lower expression of MuERVL, MuLV, IAP, MusD, and MMERGLN in the livers of G1 *Tert$^{-/-}$* mice compared to WT mice (Fig EV3B). Notably, ENU significantly upregulated MMERGLN in the livers of WT mice, but not in those of G1 *Tert$^{-/-}$* mice (Fig 4B). We then performed GO analyses between WT and G1 *Tert$^{-/-}$* mice both under control (saline) and ENU treatment and found significant upregulation for GO terms associated with viral defence and interferon response in WT mice, especially under ENU treatment, compared to G1 *Tert$^{-/-}$* mice (Fig 4C). In addition, RNA-seq analysis revealed that the expression of interferon-related genes was significantly upregulated by ENU in WT mice but not in G1 *Tert$^{-/-}$* mice (Fig 4D). Furthermore, we performed cytokine/chemokine array analysis and observed that ENU significantly upregulated cytokine/chemokine expression in WT mice, but not in G1 *Tert$^{-/-}$* mice (Fig 4E). It has previously reported that there is a positive feedback loop between ERVs and interferon response (Cañadas *et al*, 2018). To assess the relationship between TA-ERVs and interferon response *in vivo*, we treated WT and G1 *Tert$^{-/-}$* mice using dsRNA mimics poly(I:C) and measured CXCL10 levels in their serum using ELISA. Results showed that poly(I:C) significantly induced CXCL10 expression in WT mice, but not in G1 *Tert$^{-/-}$* mice (Fig 4F). On the other hand, we measured the populations of CD4$^+$/FOXP3$^+$ cells in blood of WT and G1 *Tert$^{-/-}$* mice at baseline and upon stimulation with poly(I:C) by flow cytometry analysis. The results showed that the population of CD4$^+$ and CD4$^+$FOXP3$^+$ cells increased under poly(I:C) treatment in both WT and G1 *Tert$^{-/-}$* mice, but there is no significant difference

Figure 3. TERT activates ERVs by interacting with Sp1.

A Identification of dsRNAs activated by TERT-WT or TERT-K626A using dsRIP-seq in U2OS cells. AluYb9 and tRNA-Thr-ACG as positive and negative controls, respectively.

B Quantification of antisense/sense transcripts of ERVs activated by TERT-WT or TERT-K626A in U2OS and HeLa cells using strand-specific RT–qPCR.

C Regression analysis of the correlation between *TERT* and TA-ERVs expression in 103 tumour samples across 11 cancer types. BRCA (breast invasive carcinoma), *n* = 17. cHL (classical Hodgkin lymphoma), *n* = 5. COADREAD (colon adenocarcinoma/rectum adenocarcinoma), *n* = 6. HGSC (high-grade serous ovarian cancer), *n* = 6. KIRC (kidney renal clear cell carcinoma), *n* = 12. LIHC (liver hepatocellular carcinoma), *n* = 9. LUAD (lung adenocarcinoma), *n* = 6. OSCC (oral squamous cell carcinoma), *n* = 8. PAAD (pancreatic adenocarcinoma), *n* = 10. PRAD (prostate adenocarcinoma), *n* = 6. THCA (thyroid carcinoma), *n* = 18.

D MeDIP-qPCR analysis of TA-ERVs sites in HeLa cells ectopically expressing TERT-WT or TERT-K626A. Primer sets recognizing exon 8 of the human *ZC3H13* gene and a gene desert on chromosome 12 were used for positive and negative controls, respectively.

E ChIP-qPCR for TERT and Sp1 targets on TA-ERVs in U2OS cells with TERT ectopic expression and in HeLa cells. β-actin promoter was used as a negative control, and *VEGF* promoter was used as a positive control.

Data information: Data represent mean ± SEM of three biological replicates (B, D and E). */#$P < 0.05$, **/##$P < 0.01$, ***/###$P < 0.001$, ns, not significant. Unpaired two-tailed Student's *t*-tests were used, and asterisks indicating significance for each ERV versus β-actin in TERT-WT while hashtags indicating significance for each ERV versus β-actin in TERT-K626A in (B) and (E), one-way ANOVA with Fisher's LSD tests was used for (D).

observed in population of CD4^{+} and CD4^{+}FOXP3^{+} cells between WT and G1 *Tert*^{−/−} mice at baseline or upon stimulation with poly(I:C) (Fig EV3C and D). Thus, differences observed in

expression of ERVs and cytokine/chemokine are due to the activation of ERVs by TERT, but not differences in population of immune cells in blood. Together, these results demonstrate
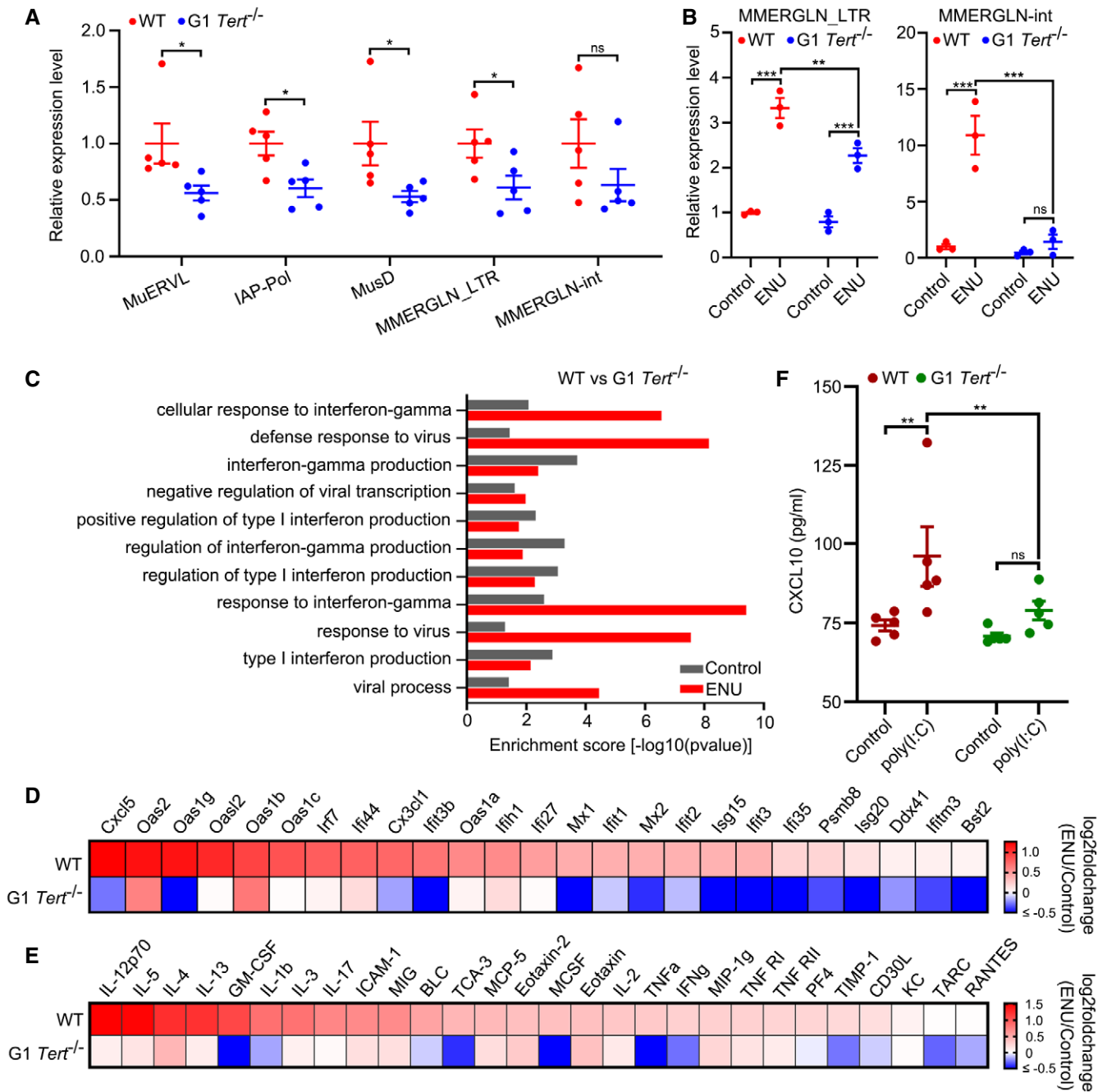
Figure 4. Deletion of *Tert* leads to decreased ERV expression and compromised interferon response in mice.

A Expression of murine ERVs in blood of WT and G1 *Tert*^{−/−} mice. *n* = 5 mice per group.

B Expression of MMERGLN_LTR and MMERGLN-int in livers of WT and G1 *Tert*^{−/−} mice treated with ENU or saline (control). *n* = 3 mice per group.

C Enriched biological processes (BP) for WT versus G1 *Tert*^{−/−} mice. GO was analysed for upregulated genes in WT mice compared to G1 *Tert*^{−/−} mice under control or ENU treatment.

D Heat map showing log2 fold change differences of interferon-related genes expression between ENU treatment and control (saline) in WT and G1 *Tert*^{−/−} mice by RNA-seq. *n* = 3 mice per group.

E Heat map showing log2 fold change differences of cytokine/chemokine between ENU treatment and control (saline) in WT and G1 *Tert*^{−/−} mice by cytokine/chemokine array. *n* = 5 mice per group.

F ELISA of CXCL10 in WT and G1 *Tert*^{−/−} mice treated with poly(I:C) or saline (control). *n* = 5 mice per group.

Data information: Data represent mean ± SEM (A, B and F). *$P < 0.05$, **$P < 0.01$, ***$P < 0.001$, ns, not significant. Unpaired two-tailed Student's *t*-tests were used for A, and two-way ANOVA with Fisher's LSD tests was used for (B) and (F).

that the absence of *Tert* compromised ERV-mediated interferon response *in vivo*.

TERT expression is associated with interferon response in tumours

By performing ssGSEA of cellular pathways in *TERT*^high and *TERT*^low tumours across TCGA, we found that in addition to "Extension of telomeres" and "Telomere maintenance", interferon-related pathways such as "Antiviral mechanism by IFN stimulated genes", "IRF3 mediated activation of type 1 IFN" and "OAS antiviral response" were significantly enriched in *TERT*^high tumours compared to *TERT*^low tumours (Fig 5A). Consistent with the results of ssGSEA, a number of interferon-related genes, including *CXCL10*, *ISG15* and *OASL,* were highly expressed in *TERT*^high tumours (Fig 5B and C). Furthermore, by an analysis of six *TERT*^low cancer types (ACC, KICH, KIRP, LGG, PRAD and THCA) and six *TERT*^high cancer types (BLCA, CESC, COAD, DLBC, LUSC and OV) across TCGA (Fig 5D), we found that *TERT*^high cancer types showed higher expression of genes related to interferon signalling, including *DDX58*, *IFIH1*, *CXCL10*, *IFI44*, *OASL* and *ISG15*, compared to the *TERT*^low cancer types (Fig 5E). In addition, we analysed *TERT* and interferon-related gene expression using the Cancer Cell Line Encyclopaedia (CCLE) (Barretina *et al*, 2012) and found that levels of *TERT* expression were closely associated with those of interferon-related genes *IFIH1*, *IFNB1*, *CXCL10*, *OASL* and *ISG20* (Fig EV4A). Consistently, results of our ssGSEA have implicated TERT in interferon response (Fig EV4B).

TERT promotes tumour immunouppression

To place our observations in a clinical context, we assessed relationship between *TERT*, ERVs and T-cell infiltration in colon tumours. Towards this, we analysed the expression of *TERT,* and LTR69, LTR38-int and MER88 in colon tumours using RT–qPCR and observed significantly positive correlation between *TERT,* and LTR69, LTR38-int and MER88 expression (Fig EV5). Notably, the expression level of *TERT* is significantly correlated with percentage of CD4^+ cells in colon tumours determined by immunohistochemistry (Fig 5F). Furthermore, we observed increased FOXP3^+ cells among CD4^+ cells in *TERT*-ERVs^high tumours, compared to

TERT-ERVs^low tumours (Fig 5G). These results indicated that *TERT* and ERV expression are associated with infiltration of CD4 T cells, especially Treg cells, in colon tumours, consistent with the results of ssGSEA for immune cell infiltration across TCGA (Fig 1A and B). In infectious diseases, the continual accumulation of Treg cells at sites of infection can upset the homeostasis of the infected organ and cause local immunosuppression and such an effect might be particularly substantial in the context of chronic systemic infection, such as with human immunodeficiency virus (HIV) or hepatitis C virus (HCV) (Belkaid & Rouse, 2005). Our data imply that the infiltration of these CD4 cells, including Th2 cells and Treg cells, contributed to an immunosuppressive microenvironment in *TERT*^high tumours, similar to a chronic virus-infected state.

The unique feature of telomerase is its low or undetectable expression in normal human somatic cells owing to transcriptional repression of the *TERT* gene during embryonic differentiation, but is reactivated in over 90% of cancerous cells by upregulation of *TERT* gene expression during cellular transformation (Cong *et al*, 2002), and high *TERT* expression is often associated with poor patient outcome (Bertorelle *et al*, 2013; Mocellin *et al*, 2013; Borah *et al*, 2015). Recent progress from our and other groups suggests a critical role for TERT in tumorigenesis, apart from its function in telomere maintenance (Park *et al*, 2009; Ghosh *et al*, 2012; Ding *et al*, 2013; Liu *et al*, 2013, 2016). Telomerase is considered as an attractive anti-cancer target (Mocellin *et al*, 2013). Therefore, understanding the mechanisms of action of telomerase in cancer development and progression would provide novel insights into the development of better therapeutic strategies.

In this study, we demonstrated that TERT-mediated ERV activation contributed to tumour immunosuppression. We found that TERT induced dsRNA expression derived from bidirectional transcription of ERVs by interacting with Sp1. Importantly, these TERT-mediated dsRNAs triggered interferon response and increased chemokine secretion in tumours. Subsequently, these chemokines attracted suppressive T-cell populations, including Th2 cells, Treg cells, NK CD56dim cells and MDSCs and established an immunosuppressive microenvironment to promote tumour progression (Fig 5H). Our findings reveal an unanticipated role for TERT as a transcriptional activator of ERVs and provide strong evidence that TA-ERV/interferon signalling contributes to immune suppression in tumours, offering insights to combinational cancer therapeutic

---

Figure 5. TERT promotes tumour immune suppression.

A   Scatterplot representing differences in ssGSEA of cellular pathways in *TERT*^high versus *TERT*^low tumours (*n* = 4,632 tumours in each group) across TCGA.

B   TCGA fragments per kilobase million (FPKM) values of *TERT, CXCL10, ISG15,* and *OASL* in tumours grouped in *TERT*^high (*n* = 500) and *TERT*^low (*n* = 500) groups. Data represent mean ± SD. *P*-values were analysed using unpaired two-tailed Student's *t*-tests.

C   TCGA FPKM values of interferon-related genes in tumours grouped in *TERT*^high (*n* = 500) and *TERT*^low (*n* = 500) groups. Heat map showing mean FPKM values of each gene.

D, E   Expression of *TERT* (D) and *DDX58*, *IFIH1*, *CXCL10*, *IFI44*, *ISG15*, and *OASL* (E) in *TERT*^high and *TERT*^low cancer types (6 types in each). ACC (adrenocortical carcinoma), *n* = 79. KICH (kidney chromophobe), *n* = 66. KIRP (kidney renal papillary cell carcinoma), *n* = 291. LGG (brain lower grade glioma), *n* = 532. PRAD, *n* = 502. THCA, *n* = 513. BLCA (bladder urothelial carcinoma), *n* = 414. CESC (cervical squamous cell carcinoma and endocervical adenocarcinoma), *n* = 306. DLBC (lymphoid neoplasm diffuse large B-cell lymphoma), *n* = 48. LUSC (lung squamous cell carcinoma), *n* = 502. OV (ovarian serous cystadenocarcinoma), *n* = 430. All boxplots include the median line, box indicates the interquartile range (IQR) and whiskers denote the 1.5 × IQR. *P*-values were analysed using two-tailed Mann–Whitney *U* test.

F   Regression analysis of the correlation between *TERT* expression and percentage of CD4^+ cells in colon tumours. *n* = 36.

G   Representative sections of immunohistochemical staining of CD4 and FOXP3 in *TERT*-ERVs^high and *TERT*-ERVs^low colon tumours. Red arrowheads indicate FOXP3^+ cells. Scale bar = 100 µm.

H   Schematic model showing TERT contributing to immunosuppressive tumour microenvironment by activating ERVs.
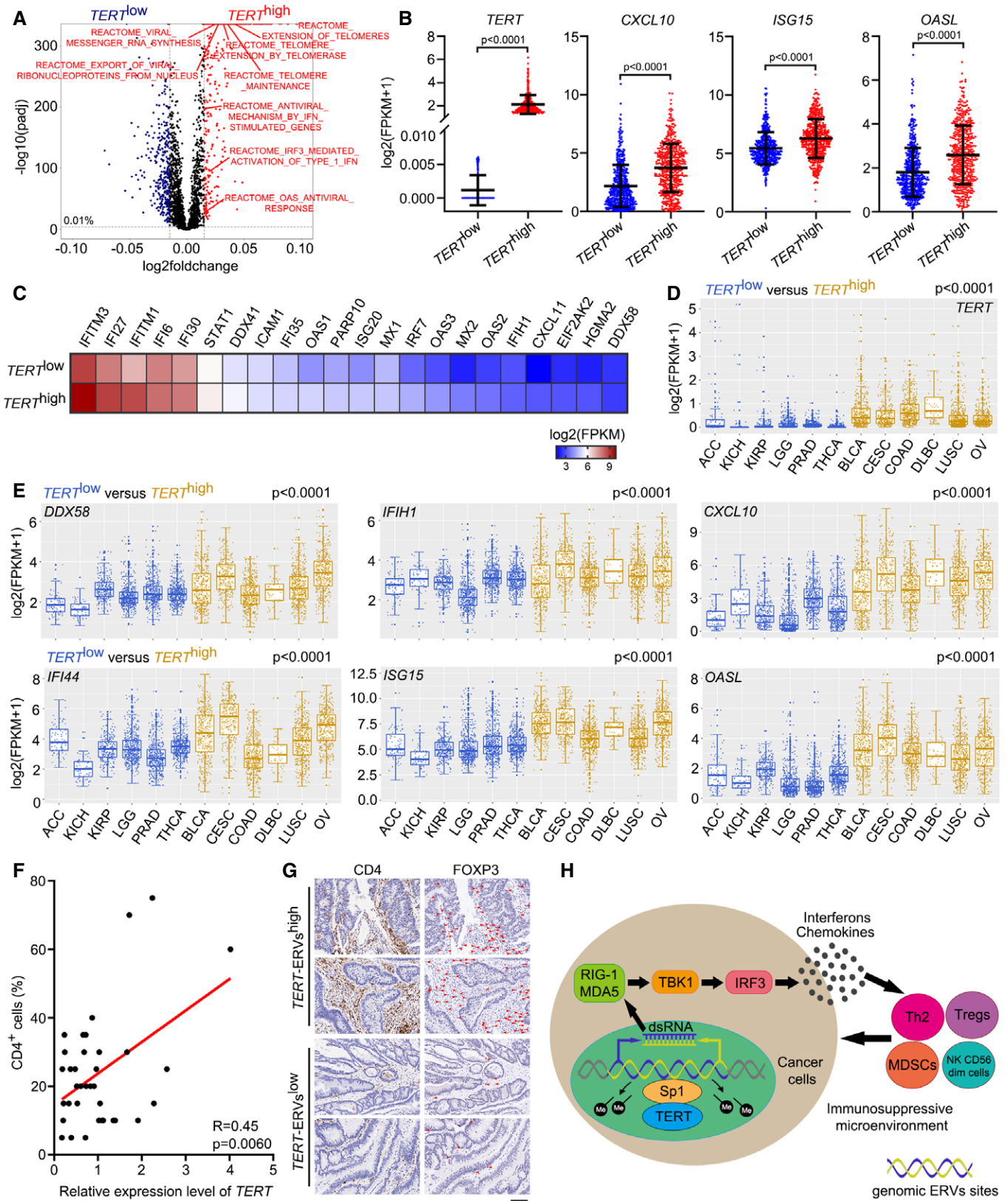
Figure 5.

strategy with telomerase inhibitors, which not only restrict cancer cell proliferation but also compromise tumour immunosuppressive microenvironments, especially for tumours highly expressing TERT.

Given that ERVs represent ~8% of the human genome (Lander *et al*, 2001) and their activation is a common feature in human cancers (Matteucci *et al*, 2018), future work on the regulation and function of ERVs in physiological and pathological contexts would provide important insights into the role of ERVs in cancer and opportunities to develop novel cancer therapeutic interventions.

Materials and Methods

Cell culture

U2OS, HeLa, WI38 and HEK293T cell lines were cultured in Dulbecco's modified Eagle's medium (DMEM) supplemented with 10% foetal bovine serum (FBS), HCT116 cells were cultured in McCoy's 5A medium (Biological Industries) with 10% FBS, at 37°C and 5% CO_2.

Plasmids and siRNAs transfection

Cells were transfected with pcDNA3.1-TERT-WT, pcDNA3.1-TERT-K626A or empty vector using Lipofectamine 3000 (Invitrogen) according to the manufacturer's instructions for 48 h.

Control siRNA (siNC), TERT and Sp1 siRNAs were purchased from GenePharma (Shanghai, China). Transfection of siRNAs was performed using Lipofectamine 3000 (Invitrogen) according to the manufacturer's instructions. The sequences of siRNAs are listed in Appendix Table S1.

Stable cell lines generation and inducing expression

GFP, TERT-WT and TERT-K626A were cloned into the pLVX-TetOne-Puro vector with the EcoRI/AgeI sites and confirmed by DNA sequencing. HEK293T cells were co-transfected with the resultant vectors, together with psPAX2 and pMD2.G. Lentiviruses were harvested, filtered and concentrated. U2OS and WI38 cells were infected with lentiviruses containing inducible GFP, TERT-WT or TERT-K626A, and stable cell lines were generated by puromycin selection. Then, the concentration of doxycycline was tested to induce the ectopic expression of TERT in U2OS and WI38 at the levels similar to that of HeLa cells. Doxycycline (Selleck) (for U2OS, 0.02 µg ml^{-1}; for WI38, 0.05 µg ml^{-1}) was added into the medium of inducible U2OS or WI38 cell lines, GFP was used as negative control. After 48 h of induction (doxycycline added every 24 h), the samples were harvested and tested.

Quantitative real-time PCR

Total RNA was extracted using TRIzol (for cell and tissue samples) or TRIzol LS (for blood samples) Reagent (Invitrogen), and the cDNA was generated using FastKing RT Kit (with gDNase) (TIANGEN) according to the manufacturer's protocol. Quantitative real-time PCR (qPCR) were performed with iTaq™ Universal SYBR Green Supermix (Bio-Rad), and *GAPDH* was measured as an internal control. Primers used for qPCR were confirmed their specificity with dissociation curves, and the sequences are listed in Appendix Table S2.

Immunofluorescence microscopy

U2OS cells transfected by TERT (WT or K626A) or vector were fixed with 3.7% paraformaldehyde and permeabilized in 0.1% Triton X-100. After blocking of nonspecific antigens with 3% goat serum, cells were incubated with primary antibody against dsRNA (J2, English and Scientific Consulting Kft., 10010200) overnight at 4°C. Then, cells were washed and subsequently incubated with secondary antibody Alexa Fluor 488 donkey anti-mouse IgG (H + L) (Invitrogen). Samples were washed and counterstained with DAPI in Vectashield mounting medium (Vectorlabs). Fluorescence was detected and imaged using a Zeiss confocal fluorescence microscope.

Telomere measurement by quantitative real-time PCR

Quantitative real-time PCR was used to measure relative telomere length based on previously described (Zhang *et al*, 2020). Genome DNA was extracted from cells using DNeasy Blood & Tissue Kit (Qiagen). Average telomere length was measured from total genomic DNA using a qPCR assay, modified for measurement of human telomeres. The qPCRs were performed using telomeric primers and primers for the reference control gene (human 36B4 single copy gene) (Appendix Table S3). For each qPCR, a standard curve was made by serial dilutions of known amounts of human genomic DNA. The telomere signal was normalized to the signal from the single copy gene to generate a T/S ratio indicative of relative telomere length.

Western blot

Protein samples were subjected to polyacrylamide gel electrophoresis using the 10% SurePAGE™ gels (GenScript), transferred to PVDF (Millipore) membranes, and immunoblotted using antibodies that specifically recognize TERT (Abcam, ab32020), TBK1 (CST, 3013), pTBK1 Ser172 (CST, 5483), IRF3 (CST, 4302), pIRF3 Ser396 (CST, 4947), Sp1 (CST, 9389), GFP (Santa Cruz, sc-9996) and GAPDH (HuaAn Biotechnology, EM1101). Secondary antibodies were Goat anti-Rabbit IgG (whole molecule) (Sigma-Aldrich, A9169) and Rabbit anti-Mouse IgG (whole molecule) (Sigma-Aldrich, A9044). Imaging of blots was performed using the Bio-Rad ChemiDoc™ MP Imaging System.

dsRNA enrichment

For dsRNA enrichment, total RNA was immunoprecipitated using the J2 dsRNA-specific antibody (English and Scientific Consulting Kft., 10010200). In brief, the product of 9 µg RNA was incubated in binding buffer (150 mM NaCl, 50 mM Tris pH 8.0, 1 mM EDTA, 1% NP-40) with 5 µg J2 antibody and 20 µl Magna ChIP™ Protein A + G Magnetic Beads (Millipore, 16-663), rotating overnight at 4°C, followed by five washes in cold binding buffer. RNA was then extracted with TRIzol Reagent and expression levels of indicated ERVs were analysed by strand-specific RNA-seq.

First-strand cDNA synthesis and strand-specific qPCR for detection of sense and antisense ERV transcripts

FastKing RT Kit (with gDNase) (TIANGEN) was adapted to perform strand-specific reverse transcription with RNA from U2OS or HeLa cells transfected by TERT (WT or K626A). For first-strand cDNA synthesis, 1 µg RNA was used for MLT1O-int, LTR69, LTR38-int, MER88, MER92C, MLT1G1-int and β-actin. A strand-specific primer (0.1 µM) for each ERV or β-actin (Appendix Table S4) was implemented in the reaction. First-strand cDNA was generated according to the manufacturer's protocol. Afterwards, strand-specific qPCR was performed with iTaq™ Universal SYBR Green Supermix (Bio-Rad). β-actin was used as internal negative control for that was previously demonstrated to have no antisense transcript (Chen et al, 2004).

MeDIP DNA preparation and qPCR

MeDIP was performed based on previously described (Morris et al, 2011). RNA-free genomic DNA was extracted from transfected HeLa cells using DNeasy Blood & Tissue Kit (Qiagen). A measure of 6 µg of each DNA sample was digested overnight at 37°C with 24 U of MseI (NEB). The reactions were stopped by heating at 65°C for 20 min, and the success of the reactions was verified by running a small aliquot of the digested DNA on an agarose gel. DNA was purified by phenol/chloroform extraction and precipitation and quantified using a NanoDrop spectrophotometer (Thermo Scientific), and 1 µg of DNA was diluted in TE buffer to a final volume of 450 µl. The DNA was denatured at 95°C for 10 min. A volume of 50 µl of 10 × IP buffer (100 mM Na-Phosphate pH 7.0, 1.4 M NaCl, 0.5% Triton X-100) and 1 µg of 5mC antibody (Epigentek, A-1014) or IgG control (CST, 5415) with 20 µl Magna ChIP™ Protein A + G Magnetic Beads (Millipore, 16-663) were added to the digested DNA, and the mixture was incubated overnight at 4°C with gentle rotation. The beads were washed three times with 1× IP buffer and resuspended in 250 µl digestion buffer (50 mM Tris pH 8.0, 10 mM EDTA, 0.5% SDS). A volume of 3.5 µl of proteinase K was added to the above mixture, and incubation was carried out 3 h at 50°C. DNA was purified by phenol/chloroform extraction and ethanol precipitation (the latter with the addition of 25 µg glycogen to facilitate visualization of the DNA pellet). 10 ng input DNA and 1 µl IP DNA were used for qPCR assay using primers listed in Appendix Table S2. Commercial primer sets recognizing exon 8 of the human ZC3H13 gene (Human Positive Control Primer Set ZC3H13, Active Motif, 71009) and a gene desert on chromosome 12 (Human Negative Control Primer Set 1, Active Motif, 71001) were used for positive and negative controls, respectively.

Chromatin immunoprecipitation (ChIP)

Chromatin immunoprecipitation (ChIP) assays were performed with a Pierce Magnetic ChIP Kit (Thermo Scientific, 26157) according to the manufacturer's instruction. Briefly, cells were crosslinked, lysed, digested with MNase and sonicated to generate DNA fragments. ChIP was performed using antibodies against TERT (Abcam, ab32020), Sp1 (CST, 9389), or normal rabbit IgG (provided by the ChIP kit) as a negative control. The immunoprecipitates were then washed and eluted. The eluates were de-crosslinked, and ChIP-enriched DNA was purified for qPCR analysis using primers listed in Appendix Table S2.

Animal studies

Tert$^{+/-}$ mice on the C57BL/6/129/SvJ genetic background were kindly provided by Dr Yie Liu (NIA, Baltimore, MD, USA). Heterozygous (Tert$^{+/-}$) pairs were intercrossed to generate first-generation Tert$^{+/+}$ (WT) and Tert$^{-/-}$ (KO) strains. All animal experiments were performed according to the guidelines of the Animal Care and Use Committee of Hangzhou Normal University. This study was compliant with all of the relevant ethical regulations regarding animal research.

For ENU treatment, age-matched WT and G1 Tert$^{-/-}$ mouse cohorts were treated with 150 µg g^{-1} ENU (Sigma-Aldrich) or saline by intraperitoneal, serum or livers were extracted after 24 h of injection.

For poly(I:C) treatment, age-matched WT and G1 Tert$^{-/-}$ mouse cohorts were treated with 50 µg poly(I:C) HMW (InvivoGen) or saline by intraperitoneal, serum was extracted after 24 h of injection.

ELISA and cytokine array

WT and G1 Tert$^{-/-}$ mice were treated with poly(I:C) or saline and serum was extracted as described above, Mouse CRG-2 (CXCL10) ELISA Kit (RayBiotech, ELM-CRG2) was used according to the manufacturer's instruction. For the ELISA of cell culture supernatant, cell culture supernatant was collected after 48 h of treatment. Human IP-10 (CXCL10) ELISA Kit (RayBiotech, ELH-IP10/IQH-IP10) and IFNβ ELISA Kit (R&D, DIFNB0) were used according to the manufacturer's instruction.

For cytokine/chemokine array, WT and G1 Tert$^{-/-}$ mice were treated with ENU or saline and serum was extracted as described above. Quantibody® Mouse Inflammation Array 1 (RayBiotech, QAM-INF-1) was used according to manufacturer's instructions.

Flow cytometry analysis

The peripheral blood mononuclear cells (PBMCs) from mouse blood were isolated using Mouse Peripheral Blood Mononuclear Cells Separation Kit (Solarbio) according to the manufacturer's instruction. Mouse PBMCs were stained with FITC Rat Anti-Mouse CD4 (BD Pharmingen, 553650), PE Rat anti-Mouse FOXP3 (BD Pharmingen, 563101), or isotype IgG control antibodies (BD Pharmingen, 554688 and 554689) for flow cytometry analysis. Briefly, cells were firstly stained with CD4-FITC or FITC isotype control. After washed, the cells were fixed and permeabilized, then stained with FOXP3-PE or PE isotype control. After washed, the cells were resuspended in PBS and analysed on a BD LSRFortessa. Fluorescence intensity of CD4 and FOXP3 was normalized to isotype controls. The data analyses were performed with FlowJo software.

Library preparation for transcriptome sequencing

A total amount of 3 µg RNA per sample was used as input material for the RNA sample preparations. Sequencing libraries were generated using NEBNext® Ultra™ RNA Library Prep Kit for Illumina®

(NEB) following manufacturer's recommendations and index codes were added to attribute sequences to each sample. Briefly, mRNA was purified from total RNA using poly-T oligo-attached magnetic beads. Fragmentation was carried out using divalent cations under elevated temperature in NEBNext First Strand Synthesis Reaction Buffer (5×). First-strand cDNA was synthesized using random hexamer primer and M-MuLV Reverse Transcriptase (RNase H⁻). Second strand cDNA synthesis was subsequently performed using DNA polymerase I and RNase H. Remaining overhangs were converted into blunt ends via exonuclease/polymerase activities. After adenylation of 3' ends of DNA fragments, NEBNext Adaptor with hairpin loop structure were ligated to prepare for hybridization. In order to select cDNA fragments of preferentially 250–300 bp in length, the library fragments were purified with AMPure XP system (Beckman Coulter). Then 3 μl USER Enzyme (NEB) was used with size-selected, adaptor-ligated cDNA at 37°C for 15 min followed by 5 min at 95°C before PCR. Then, PCR was performed with Phusion High-Fidelity DNA polymerase, Universal PCR primers and Index (X) Primer. At last, PCR products were purified (AMPure XP system) and library quality was assessed on the Agilent Bioanalyzer 2100 system.

Clustering and sequencing

The clustering of the index-coded samples was performed on a cBot Cluster Generation System using TruSeq PE Cluster Kit v3-cBot-HS (Illumia) according to the manufacturer's instructions. After cluster generation, the library preparations were sequenced on an Illumina Hiseq platform and 125 bp/150 bp paired-end reads were generated.

RNA-seq analysis for expression of genes

Raw data (raw reads) of fastq format were firstly processed through in-house perl scripts. In this step, clean data (clean reads) were obtained by removing reads containing adapter, reads containing poly-N and low quality reads from raw data. At the same time, Q20, Q30 and GC content of the clean data were calculated. All the downstream analyses were based on the clean data with high quality.

Reference genome and gene model annotation files were downloaded from genome website directly. Index of the reference genome was built using Hisat2 and paired-end clean reads were aligned to the reference genome using Hisat2 (Kim *et al*, 2015). HTSeq (Anders *et al*, 2015) was used to count the reads numbers mapped to each gene. And then FPKM of each gene was calculated based on the length of the gene and reads count mapped to this gene. Differential expression analyses of two conditions/groups were performed using the DESeq2 R package (Love *et al*, 2014). The resulting *P*-values were adjusted using the Benjamini and Hochberg's approach for controlling the false discovery rate. Genes with an adjusted *P*-value < 0.05 found by DESeq2 were assigned as differentially expressed.

GO enrichment analysis of differentially expressed genes

Gene Ontology (GO) enrichment analysis of differentially expressed genes was implemented by the clusterProfiler R package (Yu *et al*, 2012), in which gene length bias was corrected. GO terms with corrected *P*-value less than 0.05 were considered significantly enriched by differential expressed genes.

RNA-seq analysis for expression of ERVs

To assess the expression levels of ERVs, RNA-seq clean reads were mapped to the hg38 or mm10 genome using the STAR aligner software (Dobin *et al*, 2013), allowing up to three mismatches and filtering out reads that mapped to > 500 positions in the genome. Mapped files were then processed using the makeTagDirectory script of HOMER with the -keepOne option (Heinz *et al*, 2010). The tag directories of the mapped files were analysed using the analyzeRepeats.pl script of HOMER with the option 'repeat' and -noadj or -fpkm. This script adds the reads that map to multiple loci to the expression of the repeat class they represent regardless of where they are specifically placed. Differential repeats (ERVs included) expression analyses were performed using DESeq2.

Single-sample gene set enrichment analysis (ssGSEA)

The ssGSEA (Barbie *et al*, 2009) was introduced to quantify the relative infiltration of 25 immune cell types in the tumour microenvironment for 9,264 tumour samples from 24 cancer types in TCGA database (Rahman *et al*, 2015). Feature gene panels for each immune cell type were obtained from recent publications (Bindea *et al*, 2013; Charoentong *et al*, 2017). The relative abundance of each immune cell type was represented by an enrichment score in ssGSEA analysis using GSVA R package (Hänzelmann *et al*, 2013).

For ssGSEA of GO or cellular pathways, GMT files (GO: Gene Ontology gene sets and CP: Canonical pathways) were downloaded from Molecular Signatures Database on GSEA website and ssGSEA analyses were performed by GSVA R package (Hänzelmann *et al*, 2013).

RNA-seq analysis for expression of genes and ERVs from the GEO database

Published raw data of RNA-seq were downloaded from the GEO database (Accession numbers are listed in Appendix Table S5). Analyses for expression of genes and ERVs were performed as described above.

ChIP-seq analysis

Published ChIP-seq raw data for TERT (A2780: GSM2044817; HCT116: GSM2044819; VA13: GSM2154981, GSM2154982) and Sp1 (K562: GSM803505; HEK293: GSM4141459, GSM4141460; HepG2: GSM2797629) were downloaded from the GEO database. The raw data of the ChIP-seq libraries were mapped to hg38 genome using Bowtie2 with parameter --local -k 1 (Langmead & Salzberg, 2012). Average binding plots were generated using ngs.plot (Shen *et al*, 2014).

Colon tumour samples and tissue microarrays

The cDNA and tissue microarrays of human colon tumour samples were purchased from Shanghai Outdo Biotechnology. Immunohistochemical staining was performed with primary antibodies against CD4 (Abcarta, PA285) and FOXP3 (CST, 12653).

Statistical analysis

All graphs depict mean ± SEM unless otherwise indicated. Tests for differences between two groups were performed using two-tailed unpaired Student's *t*-test or two-tailed Mann–Whitney *U* test, as specified in the figure legends. One-way or two-way analysis of variance (ANOVA) was performed where applicable using the Fisher's LSD test. *P* values were considered significant if less than 0.05. Statistical significance was defined as */#$P < 0.05$, **/##$P < 0.01$, ***/###$P < 0.001$, or ns, not significant. GraphPad Prism 8 or R were used for statistical analysis of experiments, data processing, and presentation.

Data availability

RNA-seq data are available in the GEO database with GSE169715 (https://www.ncbi.nlm.nih.gov/geo/query/acc.cgi?acc=GSE169715).

Expanded View for this article is available online.

Author contributions
Jian Mao: Conceptualization; Investigation; Writing—original draft. **Qian Zhang:** Conceptualization; Investigation. **Yaxiang Wang:** Investigation. **Yang Zhuang:** Investigation. **Lu Xu:** Investigation. **Xiaohe Ma:** Investigation. **Di Guan:** Investigation. **Junzhi Zhou:** Investigation. **Jiang Liu:** Investigation. **Xiaoying Wu:** Project administration. **Qian Liang:** Investigation. **Miao Wang:** Investigation. **Yu-Sheng Cong:** Conceptualization; Supervision; Funding acquisition; Investigation; Writing—review and editing.

In addition to the CRediT author contributions listed above, the contributions in detail are:

JM, QZ, and Y-SC conceived of and designed the experiments. JM and QZ performed most of the experiments and data analyses. YW, YZ, LX, XM, DG, JZ, JL, XW, and QL, MW helped with experiments. JM, QZ, and Y-SC wrote the paper.

Disclosure and competing interests statement
The authors declare that they have no conflict of interest.

References

Anders S, Pyl PT, Huber W (2015) HTSeq—a Python framework to work with high-throughput sequencing data. *Bioinformatics* 31: 166–169

Barbie DA, Tamayo P, Boehm JS, Kim SY, Moody SE, Dunn IF, Schinzel AC, Sandy P, Meylan E, Scholl C *et al* (2009) Systematic RNA interference reveals that oncogenic KRAS-driven cancers require TBK1. *Nature* 462: 108–112

Barretina J, Caponigro G, Stransky N, Venkatesan K, Margolin AA, Kim S, Wilson CJ, Lehár J, Kryukov GV, Sonkin D *et al* (2012) The Cancer Cell Line Encyclopedia enables predictive modelling of anticancer drug sensitivity. *Nature* 483: 603–607

Belkaid Y, Rouse BT (2005) Natural regulatory T cells in infectious disease. *Nat Immunol* 6: 353–360

Bertorelle R, Briarava M, Rampazzo E, Biasini L, Agostini M, Maretto I, Lonardi S, Friso ML, Mescoli C, Zagonel V *et al* (2013) Telomerase is an independent prognostic marker of overall survival in patients with colorectal cancer. *Br J Cancer* 108: 278–284

Bindea G, Mlecnik B, Tosolini M, Kirilovsky A, Waldner M, Obenauf A, Angell H, Fredriksen T, Lafontaine L, Berger A *et al* (2013) Spatiotemporal dynamics of intratumoral immune cells reveal the immune landscape in human cancer. *Immunity* 39: 782–795

Blasco MA (2005) Telomeres and human disease: ageing, cancer and beyond. *Nat Rev Genet* 6: 611–622

Borah S, Xi L, Zaug AJ, Powell NM, Dancik GM, Cohen SB, Costello JC, Theodorescu D, Cech TR (2015) Cancer. TERT promoter mutations and telomerase reactivation in urothelial cancer. *Science* 347: 1006–1010

Cañadas I, Thummalapalli R, Kim JW, Kitajima S, Jenkins RW, Christensen CL, Campisi M, Kuang Y, Zhang Y, Gjini E *et al* (2018) Tumor innate immunity primed by specific interferon-stimulated endogenous retroviruses. *Nat Med* 24: 1143–1150

Charoentong P, Finotello F, Angelova M, Mayer C, Efremova M, Rieder D, Hackl H, Trajanoski Z (2017) Pan-cancer immunogenomic analyses reveal genotype-immunophenotype relationships and predictors of response to checkpoint blockade. *Cell Rep* 18: 248–262

Chen J, Sun M, Kent WJ, Huang X, Xie H, Wang W, Zhou G, Shi RZ, Rowley JD (2004) Over 20% of human transcripts might form sense-antisense pairs. *Nucleic Acids Res* 32: 4812–4820

Chiappinelli K, Strissel P, Desrichard A, Li H, Henke C, Akman B, Hein A, Rote N, Cope L, Snyder A *et al* (2015) Inhibiting DNA methylation causes an interferon response in cancer via dsRNA including endogenous retroviruses. *Cell* 162: 974–986

Cong Y-S, Wright WE, Shay JW (2002) Human telomerase and its regulation. *Microbiol Mol Biol Rev* 66: 407–425

Ding D, Xi P, Zhou J, Wang M, Cong Y-S (2013) Human telomerase reverse transcriptase regulates MMP expression independently of telomerase activity via NF-κB-dependent transcription. *FASEB J* 27: 4375–4383

Dobin A, Davis CA, Schlesinger F, Drenkow J, Zaleski C, Jha S, Batut P, Chaisson M, Gingeras TR (2013) STAR: ultrafast universal RNA-seq aligner. *Bioinformatics* 29: 15–21

Espinet E, Gu Z, Imbusch CD, Giese NA, Büscher M, Safavi M, Weisenburger S, Klein C, Vogel V, Falcone M *et al* (2021) Aggressive PDACs show hypomethylation of repetitive elements and the execution of an intrinsic IFN program linked to a ductal cell of origin. *Cancer Discov* 11: 638–659

Feschotte C, Gilbert C (2012) Endogenous viruses: insights into viral evolution and impact on host biology. *Nat Rev Genet* 13: 283–296

Ghosh A, Saginc G, Leow SC, Khattar E, Shin EM, Yan TD, Wong M, Zhang Z, Li G, Sung W-K *et al* (2012) Telomerase directly regulates NF-κB-dependent transcription. *Nat Cell Biol* 14: 1270–1281

Gil ME, Coetzer TL (2004) Real-time quantitative PCR of telomere length. *Mol Biotechnol* 27: 169–172

Groh S, Schotta G (2017) Silencing of endogenous retroviruses by heterochromatin. *Cell Mol Life Sci* 74: 2055–2065

Guldner IH, Wang Q, Yang L, Golomb SM, Zhao Z, Lopez JA, Brunory A, Howe EN, Zhang Y, Palakurthi B *et al* (2020) CNS-native myeloid cells drive immune suppression in the brain metastatic niche through Cxcl10. *Cell* 183: 1234–1248

Hänzelmann S, Castelo R, Guinney J (2013) GSVA: gene set variation analysis for microarray and RNA-seq data. *BMC Bioinformatics* 14: 7

Heinz S, Benner C, Spann N, Bertolino E, Lin YC, Laslo P, Cheng JX, Murre C, Singh H, Glass CK (2010) Simple combinations of lineage-determining

transcription factors prime cis-regulatory elements required for macrophage and B cell identities. *Mol Cell* 38: 576–589

Hur S (2019) Double-stranded RNA sensors and modulators in innate immunity. *Annu Rev Immunol* 37: 349–375

Jia Q, Wu W, Wang Y, Alexander PB, Sun C, Gong Z, Cheng J-N, Sun H, Guan Y, Xia X *et al* (2018) Local mutational diversity drives intratumoral immune heterogeneity in non-small cell lung cancer. *Nat Commun* 9: 5361

Kim D, Langmead B, Salzberg SL (2015) HISAT: a fast spliced aligner with low memory requirements. *Nat Methods* 12: 357–360

Küry P, Nath A, Créange A, Dolei A, Marche P, Gold J, Giovannoni G, Hartung H-P, Perron H (2018) Human endogenous retroviruses in neurological diseases. *Trends Mol Med* 24: 379–394

Lander ES, Linton LM, Birren B, Nusbaum C, Zody MC, Baldwin J, Devon K, Dewar K, Doyle M, FitzHugh W *et al* (2001) Initial sequencing and analysis of the human genome. *Nature* 409: 860–921

Langmead B, Salzberg SL (2012) Fast gapped-read alignment with Bowtie 2. *Nat Methods* 9: 357–359

Liu N, Ding D, Hao W, Yang F, Wu X, Wang M, Xu X, Ju Z, Liu J-P, Song Z *et al* (2016) hTERT promotes tumor angiogenesis by activating VEGF via interactions with the Sp1 transcription factor. *Nucleic Acids Res* 44: 8693–8703

Liu Y, Snow BE, Hande MP, Yeung D, Erdmann NJ, Wakeham A, Itie A, Siderovski DP, Lansdorp PM, Robinson MO *et al* (2000) The telomerase reverse transcriptase is limiting and necessary for telomerase function *in vivo*. *Curr Biol* 10: 1459–1462

Liu Z, Li Q, Li K, Chen L, Li W, Hou M, Liu T, Yang J, Lindvall C, Björkholm M *et al* (2013) Telomerase reverse transcriptase promotes epithelial-mesenchymal transition and stem cell-like traits in cancer cells. *Oncogene* 32: 4203–4213

Love MI, Huber W, Anders S (2014) Moderated estimation of fold change and dispersion for RNA-seq data with DESeq2. *Genome Biol* 15: 550

Manghera M, Douville RN (2013) Endogenous retrovirus-K promoter: a landing strip for inflammatory transcription factors? *Retrovirology* 10: 16

Matteucci C, Balestrieri E, Argaw-Denboba A, Sinibaldi-Vallebona P (2018) Human endogenous retroviruses role in cancer cell stemness. *Semin Cancer Biol* 53: 17–30

Mi S, Lee X, Li X-P, Veldman GM, Finnerty H, Racie L, LaVallie E, Tang X-Y, Edouard P, Howes S *et al* (2000) Syncytin is a captive retroviral envelope protein involved in human placental morphogenesis. *Nature* 403: 785–789

Mocellin S, Pooley KA, Nitti D (2013) Telomerase and the search for the end of cancer. *Trends Mol Med* 19: 125–133

Morris MR, Ricketts CJ, Gentle D, McRonald F, Carli N, Khalili H, Brown M, Kishida T, Yao M, Banks RE *et al* (2011) Genome-wide methylation analysis identifies epigenetically inactivated candidate tumour suppressor genes in renal cell carcinoma. *Oncogene* 30: 1390–1401

Park J-I, Venteicher AS, Hong JY, Choi J, Jun S, Shkreli M, Chang W, Meng Z, Cheung P, Ji H *et al* (2009) Telomerase modulates Wnt signalling by association with target gene chromatin. *Nature* 460: 66–72

Rahman M, Jackson LK, Johnson WE, Li DY, Bild AH, Piccolo SR (2015) Alternative preprocessing of RNA-Sequencing data in The Cancer Genome Atlas leads to improved analysis results. *Bioinformatics* 31: 3666–3672

Roulois D, Loo Yau H, Singhania R, Wang Y, Danesh A, Shen S, Han H, Liang G, Jones P, Pugh T *et al* (2015) DNA-demethylating agents target colorectal cancer cells by inducing viral mimicry by endogenous transcripts. *Cell* 162: 961–973

Shen L, Shao N, Liu X, Nestler E (2014) ngs.plot: Quick mining and visualization of next-generation sequencing data by integrating genomic databases. *BMC Genom* 15: 284

Strissel PL, Ruebner M, Thiel F, Wachter D, Ekici AB, Wolf F, Thieme F, Ruprecht K, Beckmann MW, Strick R (2012) Reactivation of codogenic endogenous retroviral (ERV) envelope genes in human endometrial carcinoma and prestages: Emergence of new molecular targets. *Oncotarget* 3: 1204–1219

Vargiu L, Rodriguez-Tomé P, Sperber GO, Cadeddu M, Grandi N, Blikstad V, Tramontano E, Blomberg J (2016) Classification and characterization of human endogenous retroviruses; mosaic forms are common. *Retrovirology* 13: 7

Wu Y, Qi X, Gong L, Xing G, Chen M, Miao L, Yao J, Suzuki T, Furihata C, Luan Y *et al* (2012) Identification of BC005512 as a DNA damage responsive murine endogenous retrovirus of GLN family involved in cell growth regulation. *PLoS One* 7: e35010

Yu G, Wang L-G, Han Y, He Q-Y (2012) clusterProfiler: an R package for comparing biological themes among gene clusters. *OMICS* 16: 284–287

Zhang Q, Liu N, Bai J, Zhou QI, Mao J, Xu LU, Liu J, Wei H, Ren C, Wu X *et al* (2020) Human telomerase reverse transcriptase is a novel target of Hippo-YAP pathway. *FASEB J* 34: 4178–4188